Structure, Thermal and Optical Properties of elpasolite-like $(NH_4)_2KZrF_7$

S. V. Mel'nikova[a], E. I. Pogoreltsev[a,b,*], M. S. Molokeev[a,b,c], I. N. Flerov[a,b], N.M. Laptash[d]

[a] Kirensky Institute of Physics, Federal Research Center KSC SB RAS, 660036 Krasnoyarsk, Russia

[b] Siberian Federal University, 660074 Krasnoyarsk, Russia

[c] Far Eastern State Transport University, 680021 Khabarovsk, Russia

[d] Institute of Chemistry, Far Eastern Branch of RAS, 690022 Vladivostok, Russia

Email address: pepel@iph.krasn.ru

New fluoride compound $(NH_4)_2KZrF_7$ with the elpasolite structure (sp. gr. *Fm*-3*m*) was synthesized by partial cationic substitution in $(NH_4)_3ZrF_7$ cryolite. Due to small difference in ionic radii of K^+ and NH_4^+, non-equivalent crystallographic positions 8*c* and 4*b* are occupied by both cations. Investigations of thermal, optical and structural properties in a wide range of temperature revealed two phase transitions *Fm*-3*m* ↔ $P4_2/ncm$ ↔ $P4_2/nmc$ of the first order. The results obtained are discussed in comparison with the data for the previously studied related cryolite $(NH_4)_3ZrF_7$.

Keywords: Phase transition, Structure, Optical properties, Heat capacity, Entropy

1. Introduction

Among the huge number of naturally occurring fluoride compounds, there are substances with crystal lattice formed by polyhedral complexes of different coordination: $[MF_6]$, $[MF_7]$, $[MF_8]$ and $[MF_9]$ [1 - 3]. For many years, compounds with six-coordinated polyhedra having as a rule a perovskite-like structure have been most intensively studied [4-7]. Recently, the attention of researches was also attracted by fluorides with seven-coordinated anions and the general chemical formula A_xMF_7 (x = 1, 2, 3). These substances are of interest to various "exotic"

forms of complexes [MF_7] leading to the rather high instability of the structure and complicated sequence of symmetry changes in the distorted phases under temperature as well as chemical and external pressure variation.

The polyhedra [MF_7] can be realized either in the form of a monocapped trigonal prism (C_{2v} symmetry) or a pentagonal bipyramid (D_{5h} symmetry). The former is characteristic, for example, for the series of A_2TaF_7 (A: Rb, NH4, K) compounds [1, 2, 8, 9]. The latter is realized in the isostructural compounds with x=3: $A_3Zr(Hf)F_7$ (A = NH_4, K). The pentagonal bipyramidal structure of the ZrF_7 and HfF_7 anions proposed as early as 1954 [10] was later confirmed [11,12]. According to [13, 14], ammonium compounds have a cryolite-like structure with a cubic face-centered lattice (sp. gr. O_h^5 – *Fm*-3*m*, Z = 4) at room temperature, in which the pentagonal bipyramid MF_7 was assumed to be disordered over 24 equivalent orientations. Two independent tetrahedral ammonium groups were also assumed to be disordered. These results are consistent with NMR data suggesting the dynamical nature of structural disorder in $(NH_4)_3ZrF_7$ and K_3ZrF_7 [13-15].

First examination of temperature stability of initial phases in zirconium crystals revealed that with a decrease in temperature, they undergo structural transformation from cubic to orthorhombic modification in the region of 235-213K and 254-224K for ammonium and potassium compounds, respectively [15-17]. NMR studies of molecular motion and disorder in K_3ZrF_7 [17] showed that total substitution of tetrahedral molecular cation NH_4^+ by spherical K^+ leads to a reduction to 16 the number of possible orientations of the anion ZrF_7^{3-} in phase *Fm*-3*m*. Moreover, the orthorhombic phase of this crystal was also found disordered.

More recent comprehensive studies revealed that ammonium zirconium and hafnium cryolites undergo a more complex sequence of structural distortions [18-21]. Careful polarization-optical, X-ray, calorimetric and Raman investigations as well as the group-theoretical analysis have shown that $(NH_4)_3ZrF_7$ and $(NH_4)_3HfF_7$ undergo six and five reversible phase transitions, respectively, with a certain difference in the alternation of the symmetry of the distorted phases:

(Zr) *Fm*-3*m* ↔ *F*23 ↔ *Immm* ↔ *I*2/*m* ↔ ??? ↔ *P*-1 ↔2/*c*

(Hf) *Fm*-3*m* ↔ cubic ↔ *mmm* ↔ *mmm* ↔ *mmm* ↔2/*c*

Studies of Raman spectra showed that with decreasing temperature the phase transitions in the $(NH_4)_3ZrF_7$ are accompanied by the ordering of pentagonal bipyramids $(ZrF_7)^{3-}$ and the slowing down of internal vibrations of ammonium cations [21]. Thus, combining the results of structural and spectroscopic studies, one could assume that phase transitions in both ammonium cryolites are associated only with order-disorder processes in the anion sublattice. At first glance, the results of precision calorimetric experiments are consistent with the model of disordering structural units in the cubic phase. Indeed, the total entropy change $\Sigma\Delta S_i$ associated with the sequence of structural distortions is rather large: (Zr) Rln6, (Hf) Rln4 [19,20]. However, the change in entropy at each of the transformations was turned out to be significantly less than Rln2. The latter circumstance can be commented using the following assumptions. First, the number of orientations of the polyhedron $[MeF_7]$ at transitions changes with multiplicity less than 2 (for example, Rln(24/16) = ln1.5 and so on). However, the total entropy remains very large, $\Sigma\Delta S_i$ = Rln24, compared with experimental data. Second, the disorder of structural units is "unsaturated" when cubic symmetry is preserved owing to strong anharmonicity of $(MeF_7)^{3-}$ anions vibrations without their stopping in fixed crystallographic positions. In the latter case, the entropy of the phase transition can be intermediate between the values characteristic for the displacive ($\Delta S \leq 0.1R$) and order-disorder ($\Delta S \geq 0.7R$) transformations. In the light of the above, great interest is the study of the influence of a change in chemical pressure due to partial cationic substitution $NH_4^+ \rightarrow K^+$ on the resistance to temperature of the initial cubic and distorted phases observed in $(NH_4)_3ZrF_7$ [19].

This paper presents the results of calorimetric, polarization-optical and X-ray studies of crystal $(NH_4)_2KZrF_7$.

2. Experimental

Crystalline samples of $(NH_4)_2KZrF_7$ were synthesized by mixing aqueous solutions $(NH_4)_3ZrF_7$, NH_4F and KHF_2 at a component ratio of 1: 1.5: 1.1. If the solution becomes cloudy, a few drops of hydrofluoric acid (40 % wt) should be added. The solution in a platinum cup was evaporated in a water bath until a crystalline film appeared. During cooling and continuous stirring of the solution, a plentiful fine crystalline precipitate was formed, which was washed with alcohol and air-dried. For example, 10 g $(NH_4)_3ZrF_7$ in 50 ml of H_2O, 3.0 g KHF_2 in 20 ml of H_20 and 5 ml of the NH_4F solution (40 % wt) were heated in a water bath until a crystalline film appeared on the surface of the solution. The yield of the product was about 70 %. The composition of the crystals was controlled by the content of potassium, determined by atomic absorption.

In order to check the stability of $(NH_4)_2KZrF_7$ to temperature variation, first of all, measurements of the heat capacity in a wide range of temperatures 100 - 380 K. were carried out using a DSM-10 M differential scanning microcalorimeter (DSM). The powdered compound under study was put into an aluminum sample holder. The calibration of the temperature and enthalpy scales was performed using the melting parameters of pure indium as well as tabulated data of enthalpy against temperature for Al_2O_3. The temperature was determined with an accuracy of ±1 K and the uncertainty on the enthalpy value was estimated as ±5 J mol^{-1}. Experiments were carried out in a He gaseous atmosphere using heating and cooling runs with a rate of temperature change $dT/d\tau$ of 2 to 8 K/min. Heat capacity $C_p(T)$ measurements were performed on several samples from the same crystallization experiment. The mass of the samples was about 0.06–0.10 g.

At the second stage of $(NH_4)_2KZrF_7$ characterization, optical studies were performed using an Axioskop-40 polarization microscope and a Linkam LTS 350 temperature chamber in the interval 100 – 380 K. Unfortunately, using synthesis described above, it was impossible to grow crystals with the size more than 100 μm. However, this did not prevent us to observe changes in the optical anisotropy of crystals as grown with well-developed opposite faces $(111)_c$.

The powder diffraction data of $(NH_4)_2KZrF_7$ for structural analysis were collected in the temperature range of 303-368 K (5 K step) with a Bruker D8 ADVANCE powder diffractometer (Cu-Kα radiation), TTK 450 Anton Paar heat attachment and linear VANTEC detector. The 2θ range of 5-140º was measured with 0.6 mm divergence slit, the step size of 2θ was 0.016°, and the counting time was 0.6 s per step. Additional 15 XRD patterns were measured in the temperature range of 329-348 K upon cooling with short 2θ range of 30-33.5º, 2mm divergence slit, the step size of 2θ was 0.016°, and the counting time was 1 s per step, in order to resolve the system of superstructure peaks. Moreover, 13 XRD patterns were measured in the temperature range of 332-343 K upon heating with the same short 2θ range of 30-33.5º.

3. Results and Discussion

No anomalous behavior of heat capacity was detected below room temperature. Fig. 1a demonstrates that in the process of heating above room temperature with $dT/d\tau$ = 8 K/min, we have found two anomalies of the excess heat capacity ΔC_p, at $T_1\uparrow$ = 332.5 K ± 1.0 K and $T_2\uparrow$ = 329.2 K ± 1.0 K (Fig. 1a), which was determined as a difference between the total heat capacity C_p and non-anomalous lattice contribution C_{lat}. However, upon cooling only one peak of ΔC_p was detected at $T_{1,2}\downarrow$ = 327.2 K ± 1.0 K (Fig. 1b). With repeated thermal cycling, the same behaviour of the heat capacity was observed. A similar phenomenon was found to be characteristic for all scanning speeds used for all samples studied.

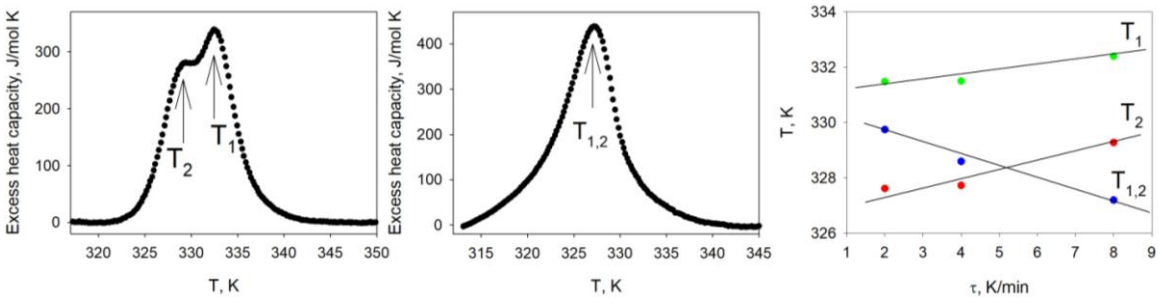

a) b) c)

Figure. 1. Temperature dependences of excess heat capacity during (a) heating and (b) cooling at $dT/d\tau$ = 8 K/min. (c) Dependence of the phase transition temperatures on the rate of heating and cooling.

Let us consider this effect in more detail. Fig. 1c shows the influence of the heating and cooling rate on temperatures of the maximum value of ΔC_p considered as the phase transition temperatures. It is seen that the decrease in heating rate is accompanied by a decrease in both temperatures, $T_1\uparrow$ and $T_2\uparrow$. Upon cooling, the temperature $T_{1,2}\downarrow$changes rapidly, decreasing with increasing $dT/d\tau$.

This behaviour of the temperature anomalies allows us to assume that upon heating $(NH_4)_2KZrF_7$ undergoes two successive phase transitions of the first order. Upon cooling, due to different thermal hysteresis $\delta T_1\uparrow$ and $\delta T_2\uparrow$, the temperature range of the intermediate phase narrows and the total structural distortions associated with two transformations detected upon heating, take place in very narrow range. Due to restrictive sensitivity of the DSM and dynamic regime of the measurements, it is not possible to detect the difference between $T_1\downarrow$and $T_2\downarrow$ and only one anomaly of ΔC_p is observed at $T_{1,2}\downarrow$.

This hypothesis can be checked by comparison of the total integral thermodynamic parameter, namely enthalpy, associated with total structural changes and determined in the heating and cooling mode. The enthalpy change associated with the two successive transformations was determined by integration of the square under peaks of the excess heat capacity. Within the experimental error, this value was found to be the same for heating and cooling processes: $\Delta H_{1\text{-}2} = \int \Delta C_p dT = 2700 \pm 300$ J mol^{-1}. Thus, the above assumptions about the behavior of temperatures $T_1\uparrow$, $T_2\uparrow$ and $T_{1,2}\downarrow$ look quite reasonable.

In polarizing-optical experiments at room temperature, bright extincting bands similar to 120° twins are observed in samples with well-developed opposite faces $(111)_c$ (Fig. 2a). This indicates the presence of a weak optical anisotropy in the crystal. Similar to DSM studies, no phase transitions below room temperature were found. When $(NH_4)_2KZrF_7$ is cooled, the intensity of light bands increases, and in the process of heating it gradually decreases. When heated above room

temperature, the crystal becomes optically isotropic at 331 K (Fig. 2b), i.e., it passes into the cubic phase. Upon subsequent cooling, optical twins reappear at 326 K.

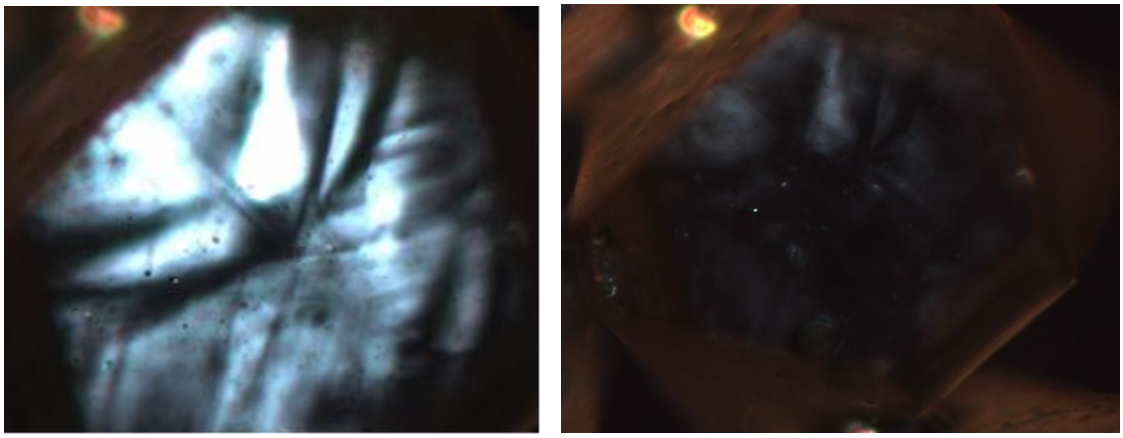

a) b)

Figure 2. Observation of twinning in polarized light of $(NH_4)_2KZrF_7$ crystal plates $(111)_c$: a) T = 295K; b) T = 331K.

Due to the absence of the anomalous behaviour of the thermal and optical properties below room temperature, XRD experiments were performed in the high temperature region including the temperatures T_1 and T_2.

All peaks of the high-temperature phase obtained at 368 K were indexed by cubic *Fm*-3*m* cell with parameters close to elpasolite $(NH_4)_3Ti(O_2)F_5$ [22, 23] and slightly smaller than the parameters of $(NH_4)_3ZrF_7$ [18]. Therefore $(NH_4)_3Ti(O_2)F_5$ crystal structure was taken as starting model for Rietveld refinement in Topas 4.2 [24]. Both N1 and N2 sites were occupied by N/K mixed ions with refined occupancies and linear restriction occ(N)+occ(K)=1 for all sites. Occupancies of F and H ions were used from $(NH_4)_3ZrF_7$ model and were not refined. The coordinates of H atoms were also fixed. Refinement was stable and gave low *R*-factors (Table 1, Fig. 3a). The coordinates of other atoms and the main bond lengths are in Table 2 and Table 3, respectively. Crystal structure is depicted in Fig. 3b. Chemical formula from refinement can be written as $[(NH_4)_{0.672(7)}K_{0.328(7)}]_2[(NH_4)_{0.732(9)}K_{0.268(2)}]ZrF_7$ or in summary

$(NH_4)_{2.08(2)}K_{0.92(2)}ZrF_7$. Thus, crystallographic positions inside the octahedron, 4b, and in the interoctahedral cavity, 8c, are occupied by both potassium atoms and ammonium groups.

The crystallographic data are deposited in Cambridge Crystallographic Data Centre (CCDC # 1912121). The data can be downloaded from the site (www.ccdc.cam.ac.uk/data_request/cif).

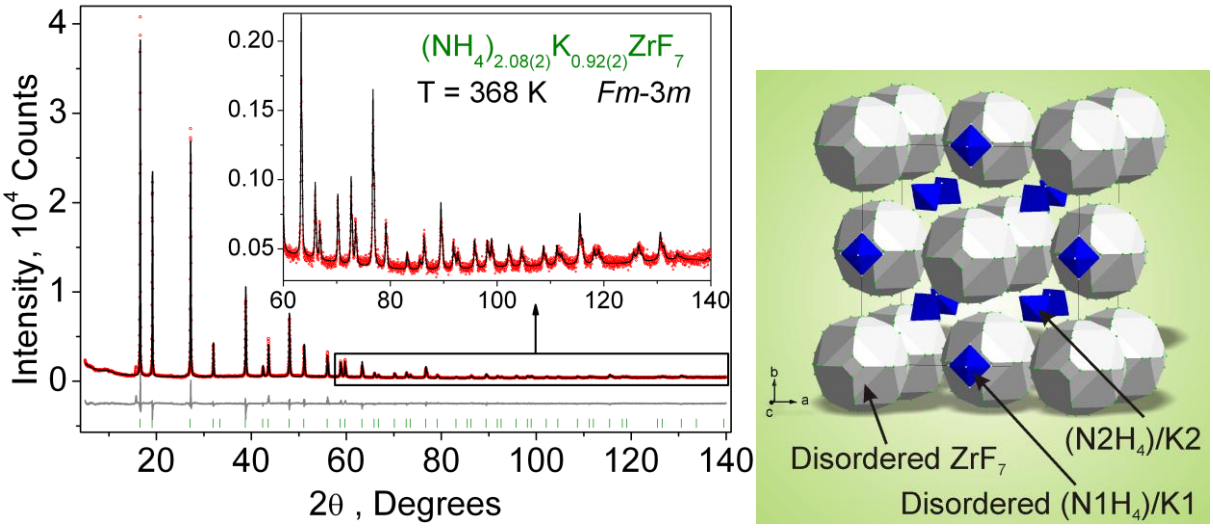

a) **b)**

Figure 3. (a) Difference Rietveld plot of $(NH_4)_2KZrF_7$ (*Fm*-3*m*) at 368 K. (b) Crystal structure of $(NH_4)_2KZrF_7$.

Cooling and heating of the sample revealed the reversible appearance and disappearance of superstructure peaks of two different systems (Fig. 4a and b). Upon cooling, first superstructure peak (1/2 3/2 3/2) appeared at T_1 = 339 ±2 K which is associated with the phase transition from *Fm*-3*m* phase. This transformation can be described by the emergence of instability at (1/2, 0, 0) (DT) of the Brillouin zone of the high-symmetry *Fm*-3*m* unit cell (hereinafter the designation of irreducible representations (irrep) and points of the Brillouin zone are given in accordance with reference books) [25, 26].

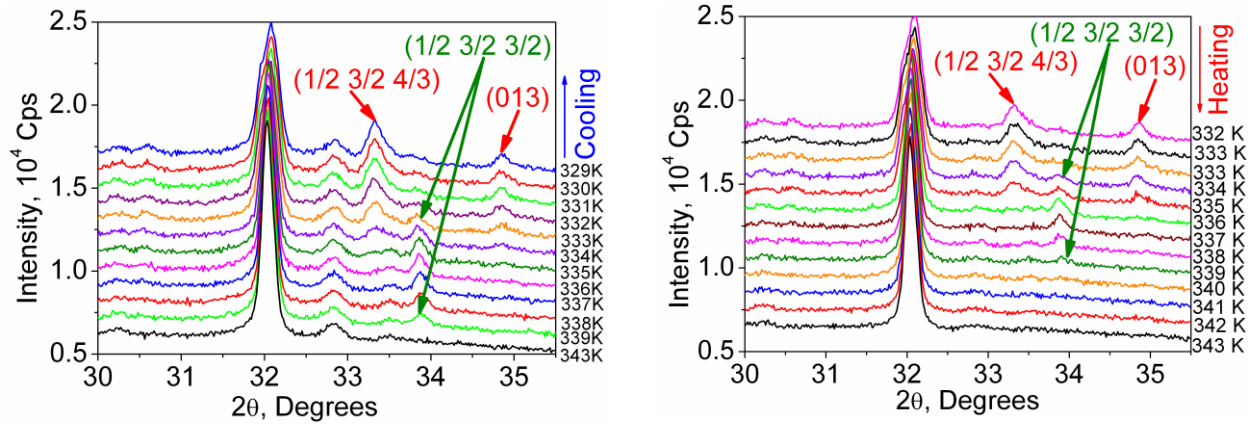

a) **b)**

Figure 4. a) Series of X-ray powder patterns in narrow 2θ range upon cooling from 343 K down to 329 K. Superstructure peak (1/2 3/2 3/2) appeared at 339 K which means phase transition from *Fm*-3*m* phase and disappeared at 333 K with simultaneous appearance of two another superstructure peaks (1/2 3/2 4/3) and (0 1 3) which means second phase transition between two distorted phases. b) The same XRD data upon heating.

It was found that the main peaks, especially (3 1 1), are slightly broadened below T_1 which may be associated with the tetragonal symmetry and Le Bail fitting ideally fitted powder pattern by tetragonal phase. Therefore, it was decided to find tetragonal phase among all isotropic subgroups of irreps DT1, DT2, DT3, DT4 and DT5. Only one space group $P4_2/ncm$ fulfill all these requirements and DT2 with (a, -a; 0, 0; 0, 0) order parameters is critical irrep which drives the phase transition *Fm*-3*m* ↔ $P4_2/ncm$. All superstructure peaks were indexed with integer (h k l) indexes and profile fitting gave good results (Table 1, Fig. 1S). The crystal structure was not solved due to the large unit cell volume, numerous refinement parameters and the disordering of the ZrF_7 polyhedron.

Further cooling leads to the disappearance of superstructure peak (1/2 3/2 3/2)at $T_2\downarrow$= 333 ±2 K and the simultaneous appearance of new peaks (1/2 3/2 4/3) and (0 1 3). In this case, the phase transition can be associated with the emergence of instability at (1/3, 0, 0) (DT) of the Brillouin zone of the high-symmetry *Fm*-3*m* unit cell. The main peak splitting (Table 1S) also can be very well fitted by tetragonal phase. The DT3 irrep with (b, $3^{1/2}$b; 0, 0; 0, 0) order parameters drives this phase transition and leads to $P4_2/nmc$ space group which is the highest among

the possible tetragonal isotropy groups in this case. Profile fitting also was successful and gave low *R*-factors (Table 1, Fig. 1S). Crystal structure $P4_2/nmc$ was also not solved/refined for the reasons mentioned above.

Temperature dependences of parameters and volume of the unit cells in all phases are presented in Fig. 5a and b. Both Figures clearly indicate two phase transitions in $(NH_4)_2KZrF_7$.

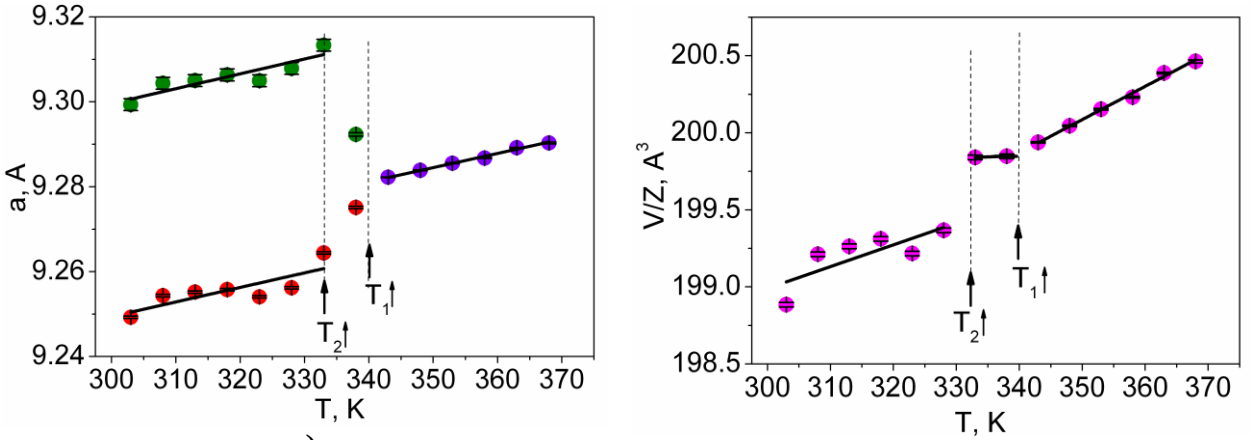

Figure 5. Temperature behaviour of (a) cell parameters: *a* for *Fm*-3*m*, $a\times2^{1/2}$ and *c*/2 for $P4_2/ncm$, $a\times2^{1/2}$ and *c*/3 for $P4_2/nmc$ phases and (b) cell volume *V*/*Z*. Temperatures T_1 and T_2 depicts the phase transition temperatures between *Fm*-3*m*, $P4_2/ncm$ and $P4_2/nmc$ phases.

Table 1. Main parameters of processing and refinement of the sample $(NH_4)_2KZrF_7$ in *Fm*-3*m*, $P4_2/ncm$ and $P4_2/nmc$ phases

T, K	368	338	303
Sp.Gr.	*Fm*-3*m*	$P4_2/ncm$	$P4_2/nmc$
a, Å	9.2904 (2)	6.5585 (2)	6.5402 (2)
c Å	–	18.5846 (8)	27.898 (1)
V, Å^3	801.87 (4)	799.39 (6)	1193.31 (9)
Z	4	4	6
2θ-interval, °	5-140	5-140	5-140
R_{wp}, %	7.7	6.36	6.67
R_p, %	5.72	4.88	5.08
R_{exp}, %	3.78	3.68	3.61
χ^2	2.05	1.73	1.85

R_B, %	3.80	–	–

Table 2. Fractional atomic coordinates and isotropic displacement parameters ($Å^2$) of $(NH_4)_2KZrF_7$ at T = 368 K

Atom	*x*	*y*	*z*	B_{iso}	Occ.
Zr	0	0	0	2.3 (1)	1
N1	0.5	0.5	0.5	1.5 (2)	0.732 (9)
K1	0.5	0.5	0.5	1.5 (2)	0.268 (9)
N2	0.25	0.25	0.25	4.0 (2)	0.672 (7)
K2	0.25	0.25	0.25	4.0 (2)	0.328 (7)
H1	0	0	0.402	5	1
H2	0.19	0.19	0.19	5	0.75
F1	0	0.0485 (5)	0.2150 (5)	2.6 (2)	0.208
F2	0	0.1444 (18)	0.1762 (16)	2.6 (2)	0.083

Table 3. Main bond lengths (Å) of $(NH_4)_2KZrF_7$ at T = 368 K

Zr—F1	2.047 (5)	F1—N1^{ii}	2.047 (5)
Zr—F2	2.12 (2)	F1—K1^{ii}	2.047 (5)
N1—H1^{i}	0.91	F2—N1^{ii}	2.12 (2)
N2—H2	0.96	F2—K1^{ii}	2.12 (2)

Symmetry codes for: (i) -*x*+1/2, -*y*+1/2, -*z*+1; (ii) -*y*+1/2, *z*-1/2.

Let’s look at the results of partial replacement of ammonium cation with potassium in cryolite $(NH_4)_3ZrF_7$. First of all, this did not lead to a change in the cubic symmetry Fm-3m of the initial high-temperature phase. At the same time, the refinement of the structure showed that the cationic substitution occurred in both non-equivalent crystallographic positions 8*c* and 4*b* that is most likely due to the rather small difference in ionic radii of K^+ and NH_4^+. It was also found that the cubic phase in the elpasolite $(NH_4)_2KZrF_7$ is less stable since the first phase transition occurs ~ 40 K higher than in cryolite [19].

While calorimetric and X-ray studies revealed two phase transitions, only one transformation to the isotropic phase was found in the optical experiments.

It is likely that the latter is due to the preservation of the tetragonal syngony during the transition at T_2. Studies of solid solutions $(NH_4)_{3-x}KxZrF_7$ with x = 0 – 1 are of interest to find out the reasons for such a strong change in the sequence of structural distortions.

It should be noted that the enthalpy value ΔH_{1-2} for elpasolite is comparable to the total enthalpy $\Sigma\Delta H_i$ = 3000 J mol^{-1} determined by the same DSM method for cryolite $(NH_4)_3ZrF_7$ undergoing six structural transformations [19]. However, the total entropy changes differ for both fluoride compounds significantly: ΔS_{1-2} = Rln2.6 and $\Sigma\Delta S_i$ = Rln6. This circumstance may be due to at least two reasons. First, due to the lower phase transition temperature from the initial cubic phase in cryolite and, second, to a smaller degree of the final structure distortions in elpasolite. For more correct information about the entropy parameters, the detailed studies of the heat capacity are need using an adiabatic calorimeter. Such studies as well as dilatometric investigations allowing to us to get important information on the peculiarities of the thermal expansion will be performed soon.

4. Conclusions

By cationic substitution of $K^+ \rightarrow NH_4^+$in the cryolite structure of $(NH_4)_3ZrF_7$ (Fm-3m, Z=4), elpasolite $(NH_4)_2KZrF_7$ with the same initial cubic symmetry was synthesized for the first time. The ionic radii of monovalent cations are rather close to each other, as a result, the non-equivalent crystallographic positions 8*c* and 4*b* are occupied by both potassium and ammonium. XRD-refined chemical formula is $[(NH_4)_{0.672(7)}K_{0.328(7)}]_2[(NH_4)_{0.732(9)}K_{0.268(2)}]ZrF_7$ or in summary $(NH_4)_{2.08(2)}K_{0.92(2)}ZrF_7$.

Calorimetric, optic and X-ray studies have shown that elpasolite undergoes two reversible first order structural transformations *Fm*-3*m* ↔ $P4_2/ncm$ ↔ $P4_2/nmc$ instead of six phase transitions with more complicated structural distortions revealed earlier by us in $(NH_4)_3ZrF_7$ [18, 19]. It was also found that the cationic substitution was manifested in a decrease in the temperature stability of

the *Fm*-3*m* phase, as well as a significant decrease in the entropy of phase transitions.

Such a strong effect of partial cationic substitution on the structure and physical properties seems unexpected, especially considering that in the K_3ZrF_7 complex, the orthorhombic phase is assumed [15, 17, 27]. In connection with the above, of undoubted interest is the study of $(NH_4)_{3-x}K_xZrF_7$ solid solutions with potassium concentrations $x < 1$.

Acknowledgements

The reported study was funded by RFBR according to the research project No. 18-02-00269 a.

The authors are grateful to Krasnoyarsk Center of collective use of SB RAS for providing X-ray analytical equipment.

References

1. Z. Mazej, R. Hagiwara. Review. Hexafluoro-, heptafluoro-, and octafluoro-salts, and $[M_nF_{5n+1}]^-$ (n = 2, 3, 4) polyfluorometallates of singly charged metal cations, Li^+–Cs^+, Cu^+, Ag^+, In^+ and Tl^+. Journal of Fluorine Chemistry 128 (2007) 423–437.

2. M. Leblanc, V. Maisonneuve, A. Tressaud, Crystal Chemistry and Selected Physical Properties of Inorganic Fluorides and Oxide-Fluorides. Chem. Rev. **115** (2015) 1191−1254.

3. J.F Scott, R. Blinc, Multiferroic magnetoelectric fluorides: why are there so many magnetic ferroelectrics? J. Phys.: Condens. Matter 23 (2011) 113202 (17pp)

4. K.S. Aleksandrov, B.V. Beznosikov. Perovskitopodobnye kristally. Nauka, Novosibirsk (1997) 216 p.

5. K.S. Aleksandrov, B.V. Beznosikov. Perovskity. Nastoyashee I budushee. Izdatelstvo SO RAN, Novosibirsk (2004) 231 p.

6. I.N. Flerov, M.V. Gorev, K.S. Aleksandrov, A. Tressaud, J. Grannec, M. Couzi, Mater. Phase transitions in elpasolites (ordered perovskites). Sci. Eng. R 24 (1998) 81–150.

7. Ch.J. Howard, B.J. Kennedy, P.M. Woodward, Ordered double perovskites – a group0-theoretical analysis. Acta Cryst. B59 (2003) 463-471.

8. R.B. English, A.M. Heyns, E.C. Reynhardt, An x-ray, NMR, infrared and Raman study of K_2TaF_7. J. Phys. C: Solid State Phys. 16 (1983) 829–840.

9. N.M. Laptash, A.A. Udovenko, T.B. Emelina. Dynamic orientation disorder in rubidium fluorotantalate. Synchronous Ta–O and Ta–F vibrations. J. Fluor. Chem. 132 (2011) 1152-1158.

10. W.H. Zachariasen. Crystal Chemical Studies of the 5f-Series of Elements. Acta Crystallogr. **7** (1954) 792-794.

11. H.J. Hurst, J.C. Taylor. The Crystal Structure of Ammonium Heptafluorozirconate and the Disorder of the Heptafluorozirconate Ion. Acta Crystallogr. B 26 (1970) 417.

12. H.J. Hurst, J.C. Taylor. A neutron diffraction analysis of the disorder in ammonium heptafluorozirconate. Acta Cryst. B26 (1970) 2136–2137.
13. A. A. Udovenko, N. M. Laptash. Orientational disprder in crystal structures of $(NH_4)_3ZrF_7$ and $(NH_4)_3NbOF_6$. J. Struct. Chem. 49 (2008) 482–488.
14. A.A. Udovenko, A.A. Karabtsov and N.M. Laptash. Crystallographic features of ammonium fluoroelpasolites: dynamic orientational disorder in crystals of $(NH_4)_3HfF_7$ and $(NH_4)_3Ti(O_2)F_5$. Acta Cryst. B73 (2017). 1–9.
15. V.P. Tarasov, Yu.A. Buslaev, Molecular movement and ZrF_7 configuration.J. Struct. Chem. 10 (1969) 816-818.
16. Yu.A. Buslaev, V.I. Pakhomov, V.P. Tarasov, V.N. Zege. F^{19}Spin – Lattice Relaxation and X-Ray Study of Phase Transition in Solid K_3ZrF_7 and $(NH_4)_3ZrF_7$. Phys. Stat. Sol. (b) 44 (1971) K13-K15.
17. E.C. Reynhardt, J.C. Pratt, A. Watton, H.E. Petch. NMR study of molecular motions and disorder in K_3ZrF_7 and K_2TaF_7. J. Phys. C: Solid State Phys. **14** (1981) 4701.
18. S.V. Misyul, S.V. Mel'nikova, A.F. Bovina, N.M. Laptash, Optical and X-ray studies of the symmetry of the distorted phases in $(NH_4)_3ZrF_7$ crystal. Phys. Solid State 50 (2008) 1951–1956.
19. V.D. Fokina, M.V. Gorev , E.V. Bogdanov , E.I. Pogoreltsev, I.N. Flerov , N.M. Laptash. Thermal properties and phase transitions in $(NH_4)_3ZrF_7$. Journal of Fluorine Chemistry 154 (2013) 1–6
20. E. Pogoreltsev, E. Bogdanov, S. Melnikova, I. Flerov, N. Laptash. $(NH_4)_3HfF_7$: Crystallooptical and calorimetric studies of a number of successive phase transitions. $(NH_4)_3HfF_7$: Journal of Fluorine Chemistry 204 (2017) 45–49.
21. A.S. Krylov, S.N. Krylova, N.M. Laptash, A.N. Vtyurin. Raman scattering study of temperature induced phase transitions in crystalline ammonium heptafluorozirconate, $(NH_4)_3ZrF_7$. Vibrational Spectroscopy 62 (2012) 258– 263.
22. Ž. Ružić-Toroš, . Kojić-Prodić, M. Šljukić. Crystal structures of trisammonium bisperoxotetrafluoroniobate (V) and analogous tantalate (V). Inorganica chimica acta, 86(3) (1984) 205-208.

23. I.N. Flerov, M.V. Gorev, V.D. Fokina, M.S. Molokeev, A.D. Vasil'ev, A.F. Bovina, N.M. Laptash. Heat capacity, structural disorder, and the phase transition in cryolite $(NH_4)_3Ti(O_2)F_5$. Physics of the Solid State, 48(8) (2006) 1559-1567.
24. Bruker AXS TOPAS V4: General profile and structure analysis software for powder diffraction data. – User's Manual. Bruker AXS, Karlsruhe, Germany. 2008.
25. O.V. Kovalev, Representations of the Crystallographic Space Groups: Irreducible Representations, Induced Representations, and Corepresentations; Gordon and Breach Science, 1993.
26. S.C. Miller, W.F. Love, Tables of irreducible representations of space groups and co-representations of magnetic space groups; Pruett Press, 1967.
27. M. T. Dova, M. C. Caracoche, A. M. Rodriguez, J. A. Martinez, P. C. Rivas, A. R. Lopez Garcia. Time-differential perturbed-angular-correlation study of phase transitions and molecular motions in $K_3(Hf,Zr)F_7$. Phys. Rev B40 (1989) 11258-11263.

Supported Information

Table 1S. The FWHM (º) of main peaks at different temperatures

T, K	(1 1 1)	(2 0 0)	(2 2 0)	(3 1 1)	(0 0 4)	(0 4 2)
368	0.111	0.122	0.143	0.163	0.201	0.211
338	0.116	0.122	0.143	0.169	0.203	0.222
303	0.117	0.196	0.174	0.263	0.389	0.354

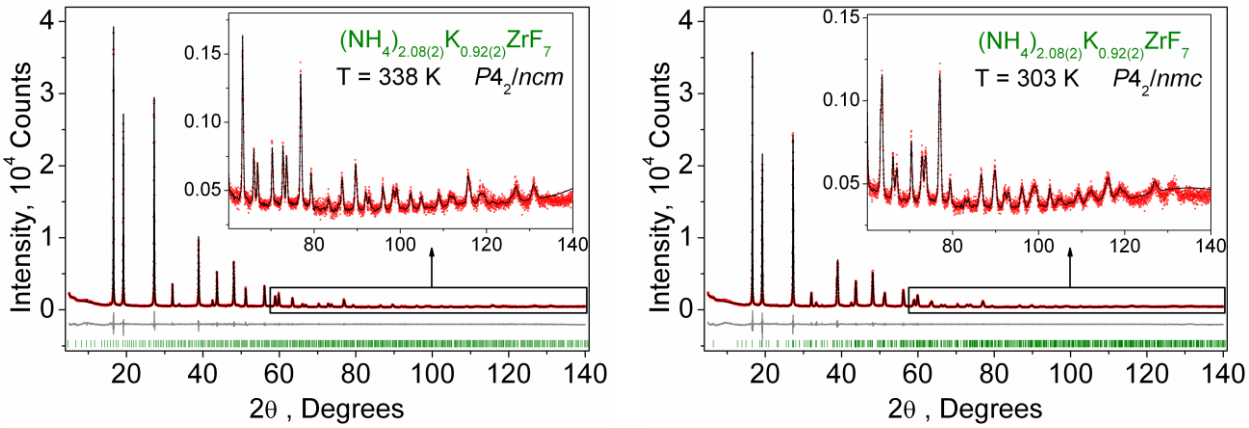

Figure 1S. Difference Rietveld plot of $(NH_4)_2KZrF_7$ at: a) 338 K ($P4_2/ncm$); b) 303 K ($P4_2/nmc$).

Table 2S. Main parameters of processing and refinement of the $(NH_4)_2KZrF_7$ sample

Temperature, K	Space group	Cell parameters (º, Å), Cell volume (Å^3)	R_{wp}, R_p, R_{exp} (%), χ^2
303	$P4_2/nmc$	a = 6.5402 (2), c = 27.898 (1), V = 1193.31 (9)	6.67, 5.08, 3.61, 1.85
308	$P4_2/nmc$	a = 6.5438 (2), c = 27.9131 (9), V = 1195.27 (8)	6.44, 4.88, 3.61, 1.78
313	$P4_2/nmc$	a = 6.5444 (2), c = 27.915 (1), V = 1195.58 (9)	6.55, 4.98, 3.61, 1.82
318	$P4_2/nmc$	a = 6.5448 (2), c = 27.919 (1), V = 1195.87 (9)	6.87, 5.14, 3.61, 1.90
323	$P4_2/nmc$	a = 6.5436 (2), c = 27.9149 (9), V = 1195.30 (9)	6.42, 4.92, 3.61, 1.78
328	$P4_2/nmc$	a = 6.5451 (2), c = 27.9236 (9), V = 1196.20 (9)	7.00, 5.29, 3.61, 1.94
333	$P4_2/nmc$	a = 6.5509 (2), c = 27.940 (1), V = 1199.04 (9)	6.74, 5.12, 3.61, 1.87
338	$P4_2/ncm$	a = 6.5585 (2), c = 18.5846 (8),	6.36, 4.88, 3.68, 1.73

		V = 799.39 (6)	
343	*Fm*-3*m*	a = 9.28222 (8), V = 799.75 (2)	6.91, 5.33, 3.77, 1.83
348	*Fm*-3*m*	a = 9.28386 (9), V = 800.18 (2)	6.37, 4.96, 3.77, 1.69
353	*Fm*-3*m*	a = 9.28554 (9), V = 800.61 (2)	6.31, 4.84, 3.77, 1.68
358	*Fm*-3*m*	a = 9.28674 (9), V = 800.92 (2)	7.12, 5.35, 3.78, 1.88
363	*Fm*-3*m*	a = 9.28916 (9), V = 801.55 (2)	7.48, 5.56, 3.78, 1.98
363	*Fm*-3*m*	a = 9.2903 (2), V = 801.85 (4)	7.77, 5.72, 3.78, 2.05